Nanoscale Res Lett (2007) 2:112–117
DOI 10.1007/s11671-007-9040-1

NANO EXPRESS

Self-assembled InAs quantum dot formation on GaAs ring-like nanostructure templates

**N. W. Strom · Zh. M. Wang · J. H. Lee ·
Z. Y. AbuWaar · Yu. I. Mazur · G. J. Salamo**

Published online: 8 February 2007
© to the authors 2007

Abstract The evolution of InAs quantum dot (QD) formation is studied on GaAs ring-like nanostructures fabricated by droplet homo-epitaxy. This growth mode, exclusively performed by a hybrid approach of droplet homo-epitaxy and Stransky-Krastanor (S-K) based QD self-assembly, enables one to form new QD morphologies that may find use in optoelectronic applications. Increased deposition of InAs on the GaAs ring first produced a QD in the hole followed by QDs around the GaAs ring and on the GaAs (100) surface. This behavior indicates that the QDs prefer to nucleate at locations of high monolayer (ML) step density.

Keywords GaAs/GaAs droplet homo-epitaxy · InAs quantum dots · Molecular beam epitaxy · Self-assembly

Introduction

In recent times, semiconductor quantum dots (QDs) have attracted increased attention because of their potential application in optoelectronic devices, such as, for quantum computation [1], lasers [2], single photon sources [3–5], charge storage devices [6] and single photon detectors [7]. Because of the need to control the size, shape, and distribution of these zero-dimensional structures, much effort has been put forth to fabricate QDs with uniformity and precision. Different methods have attempted to fulfill this task, including chemical synthesis [8], lithography [9–11], STM and AFM tip-assisted deposition [12, 13], and self-assembly [14–18]. The growth of unique complex structures such as rings, ensembles of dots, and molecules have been successfully demonstrated [16, 19, 20]. While these techniques have been quite successful, new approaches would be welcomed.

For example, in one method of self-assembly based on the Stranski–Krastanov (SK) growth mode [14, 15], lattice strain drives deposited films into three-dimensional structures. That is, in this SK-based growth mode, one material is deposited on a different material surface so that a lattice-mismatch between the two materials creates strain and drives the growth of a nanostructure. This technique, however, is limited by the available lattice mismatch, and therefore a different growth approach is needed both when using lattice-matched materials such as GaAs/GaAs and when growing nanostructures under inefficient lattice mismatch such as GaAs/$Al_xGa_{1-x}As$. A new approach called "droplet epitaxy," however, overcomes this limitation. In droplet epitaxy, a droplet of one material is deposited on a substrate and forms a nanostructure after annealing (specifically in an As_4 flux in the GaAs/AlGaAs hetero-epitaxy material [16] and GaAs/GaAs homo-epitaxy material). In the case of the GaAs/GaAs material, Ga is deposited in droplets on a GaAs substrate by molecular beam epitaxy (MBE). Specifically, the droplet formation is based on the Volmer–Weber growth mode [21]. These droplets are then subsequently exposed to an As_4 flux, forming mound structures and crystallizing to the GaAs surface. With increased As_4 flux, the mounds then diffuse, forming a nano-ring structure. Although work has been

N. W. Strom · Zh. M. Wang · J. H. Lee (✉) ·
Z. Y. AbuWaar · Yu. I. Mazur · G. J. Salamo
Department of Physics, University of Arkansas,
Fayetteville, AR 72701, USA
e-mail: jx114@uark.edu

done on the GaAs/AlGaAs hetero-material system [15, 22–24], little work has been done on the GaAs/GaAs homo-material system.

In this paper, we report on the use of ring-like nanostructures formed by droplet homo-epitaxy of GaAs/GaAs as a template for InAs QDs based on the SK growth mode. That is, we have discovered a way to form self-assembled InAs QDs using GaAs ring-like nanostructures as templates. Because the ring-like structures have a high-density of GaAs monolayer (ML) steps inside and around the holes, deposited InAs prefers to nucleate QDs along the sidewalls around and inside the holes. Here we focus on showing the progression from bare ring-like nanostructures to structures with an extensive InAs QD growth, mediated by single InAs QDs forming within the hole. This growth mode, exclusively performed by a hybrid approach of droplet homo-epitaxy and SK-based QD self-assembly, enables one to form new morphologies of QDs and single-QD structures that may find use in optoelectronic applications.

Experimental details

Each sample in our experiment was grown on epitaxy-ready 625 μm-thick GaAs (100) substrates by MBE. The surfaces were monitored with a reflection high-energy electron diffraction (RHEED) system, and the MBE system was equipped with a highly accurate solid-source valve, controlling instantaneous As_4 flux by the positioning of the As_4 valve. The oxide on each substrate was first desorbed at 580 °C for 10 min, and a 330 nm GaAs buffer was then grown at 595 °C. A 5 min annealing took place, and the temperature was gradually decreased to 540 °C. The GaAs ringed-nanostructures first formed on the surface by depositing 20 ML of Ga (a corresponding amount of GaAs after the Ga ''arsenized,'' i.e., crystallized to the surface) at 1.0 ML/sec and allowing the droplets to coagulate on the surface for 1 min 20 sec. A 1.3×10^{-6} Torr beam equivalent pressure (BEP) of As_4 was then used (valve 5% open) on the Ga droplets for 1 min 40 sec to allow the Ga to complete the ''arsenization'' process. Subsequently the growth recipe for each sample was performed at 500 °C. In this experiment, the samples consisted of 0.0, 0.8, 1.2, 1.36, 1.6, 1.76, 2.0, and 2.4 ML of InAs deposited under a 3.4×10^{-6} Torr BEP of As_4 flux (40% open) at 0.08 ML/sec. This was then followed by a 20 sec growth interruption. Finally, the temperature was gradually decreased with the As_4 valve 40% open, and the samples were then imaged by ex situ atomic force microscopy (AFM).

Results and discussion

After annealing in an As_4 flux, nanostructures formed during the different depositions of the InAs. GaAs accumulation is primarily directed towards [01-1] and less so along [011] due to the anisotropic nature of the GaAs (100) surface in fig. 1. The ring-like nanostructures retained their elongation in each sample, forming the different morphologies with the subsequent InAs deposition. The ring-like structures' highest peaks remained ~10 nm above the GaAs surface along the [01-1] and [0-11] directions from the structures' holes, as show in the profiles in Fig. 2. They were ~5 nm above the surface along the [011] and [0-1-1] directions from the holes, indicating that the InAs preferred not to deposit directly on the peaks of the nanostructures' rings until the coverage reached ~2.4 ML. Figure 1 shows $3 \times 3\ \mu m^2$ AFM images of the subsequent nanostructures that were created. The InAs deposited first in the holes of the GaAs nanostructures. The line profiling in Fig. 2 shows the progression of the morphologies with increasing InAs deposition.

The first sample is without InAs coverage, as indicated in Fig. 1a and Fig. 2a. The hole of this sample approached an average depth of 22.1 nm below the surface. The hole formation is induced by the interaction energies between the Ga droplets the GaAs surface. The details of formation mechanism of these deep holes will be discussed in other publication. Figure 1b shows how the 0.8 ML InAs coverage significantly filled in the hole, forming a 3 D region with this lower band gap material and decreasing the depth of hole to ~5 nm below the surface. Through each subsequent InAs deposition, the hole remained relatively less deep than the initial hole, at ~6 nm (±4 nm) below the surface. Figure 1c and Fig. 2c indicate that after 1.2 ML deposition, small InAs QDs formed inside the hole. We believe that the QD critical coverage in the hole is less than the typical 1.7 ML reported for planar InAs/GaAs QDs [25] due to the high density of ML steps in the hole. It appears that these QDs many times formed on the slope of the side of the hole, where the density of ML steps would be more localized, as opposed to the deepest part of the of the hole, i.e. the pit, where the ML steps would be surrounding the QD on all sides. Table 1 indicates that the average height of these QDs is only 3.1 nm, whereas the average height of the QDs in the 1.36 ML deposition is 6.0 nm.

After 1.36 ML of deposition, the InAs appeared to prefer to deposit on the previously formed InAs QDs, as the QDs appear to grow in size. However, with continued growth of the largest QD in the holes,

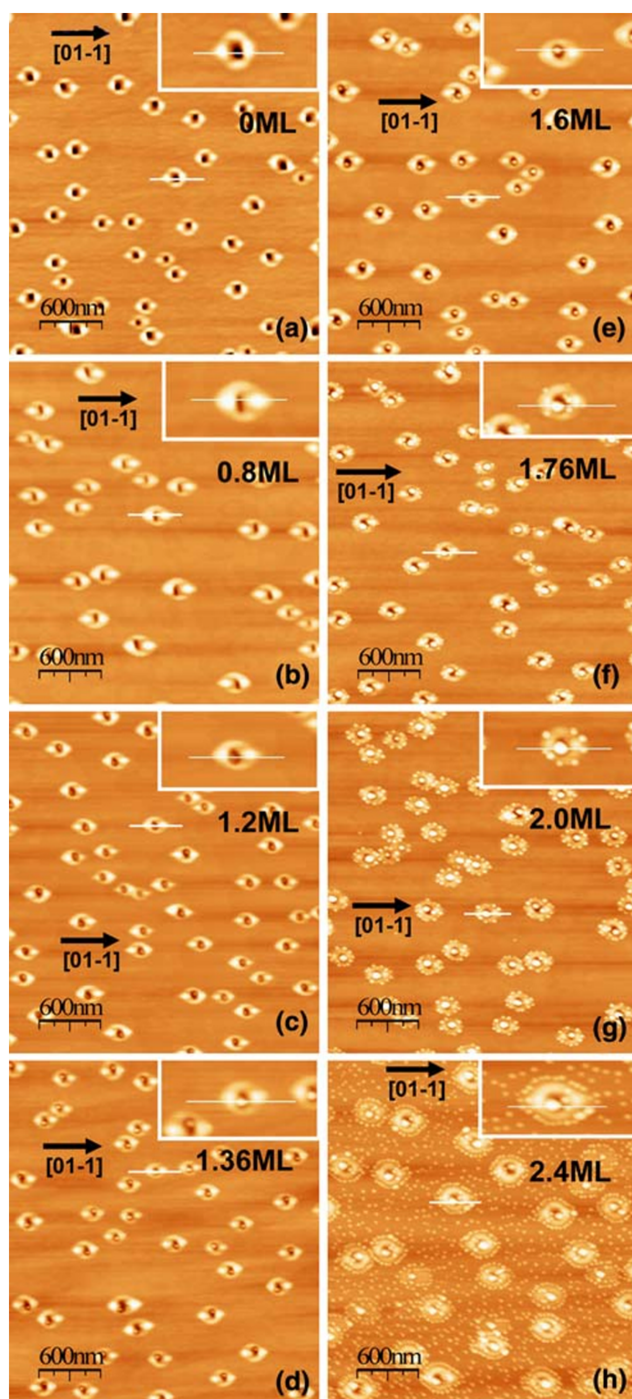

Fig. 1 Tapping mode 3×3 μm^2 AFM images of the (**a**) 0.0 ML, (**b**) 0.8 ML, (**c**) 1.2 ML, (**d**) 1.36 ML, (**e**) 1.6 ML, (**f**) 1.76 ML, (**g**) 2.0 ML, and (**h**) 2.4 ML InAs depositions, giving the crystallographic directions of each. The insets show enlarged images of typical QDs of each sample, which are profiled in Fig. 2. Color scales vary for clarity

multiple QDs appeared on the ring-like nanostructures in the 1.36 ML and 1.6 ML samples. The additional smaller QDs formed both in the holes of the structures as well as on the outside slopes of the structures in the 1.6 ML sample, as shown in Fig. 1e and Fig. 2e. It appears that multiple QDs rarely formed on the ring of the nanostructures in the 1.36 ML deposition, only at ~1 out of every 10 ring-like nanostructures, but ~1 out of every 2 ring-like nanostructures contain multiple QDs in the 1.6 ML sample. These other QDs formed more frequently with increased deposition, as in the 1.76 ML InAs sample, where ~7 QDs appear for every ring-like nanostructure. Thus at 1.76 ML deposition, there is likely similar strain relaxation, i.e. surface energies, inside and outside the holes. In this sample, the main QDs' height and diameter grow significantly, as shown in the plot in Fig. 3, as well as in Table 1 and in the line profiling in Fig. 2f.

With 2.0 ML coverage, more dots appeared along the perimeter of the ring-like nanostructures, such that there are ~13 dots per nanostructure and a density of $\sim 7 \times 10^9$ cm^{-2}. It appears that the high-density ML step regions continued to play a role in determining where the QDs preferred to nucleate, even as the dimensions of the existing main QDs continued to increase. With the 2.4 ML coverage, the InAs QDs formed extensively around the perimeter of the ring-like nanostructures. The density of QDs on the nanostructures, i.e. along the perimeter of the ring-like nanostructure as well as on the nanostructure's ‘‘body’’ itself, is ~27 per nanostructure, and the overall QD density reached $\sim 2 \times 10^{10}$ cm^{-2}, mainly because QDs also appear on the GaAs (100) surface in this sample. The number of QDs inside the holes does not appear to increase, remaining at ~2 per ring-like nanostructure, but the dimensions of those QDs inside the holes do increase, as the plot in Fig. 3 indicates. Specifically, the main QD of each ring-like nanostructure has an average height of 30.2 nm above the reconstructed surface and an average diameter of 107.9 nm, larger than the 18.7 nm height and 87.3 nm diameter with 2.0 ML coverage. The average depth of the deepest part of the nanostructure hole decreases slightly to 2.1 nm in this sample. Because more QDs formed along the reconstructed surface and the perimeter of the nanostructures, and because the sizes of the QDs and of the ring-like nanostructure peaks increased, perhaps the surface energies are similar at each of these locations. If this be the case, it appears the critical coverage for the growth of the InAs QDs on the GaAs surface is between 2.0 and 2.4 ML. The greater than typical 1.7 ML critical thickness of InAs QDs on planar GaAs (100) [25] may be due to the transport of In from the reconstructed surface to the larger QDs. Also, one of the interesting aspects of this growth sequence is that of an approximate linear increase in the QD sizes with the increasing in InAs

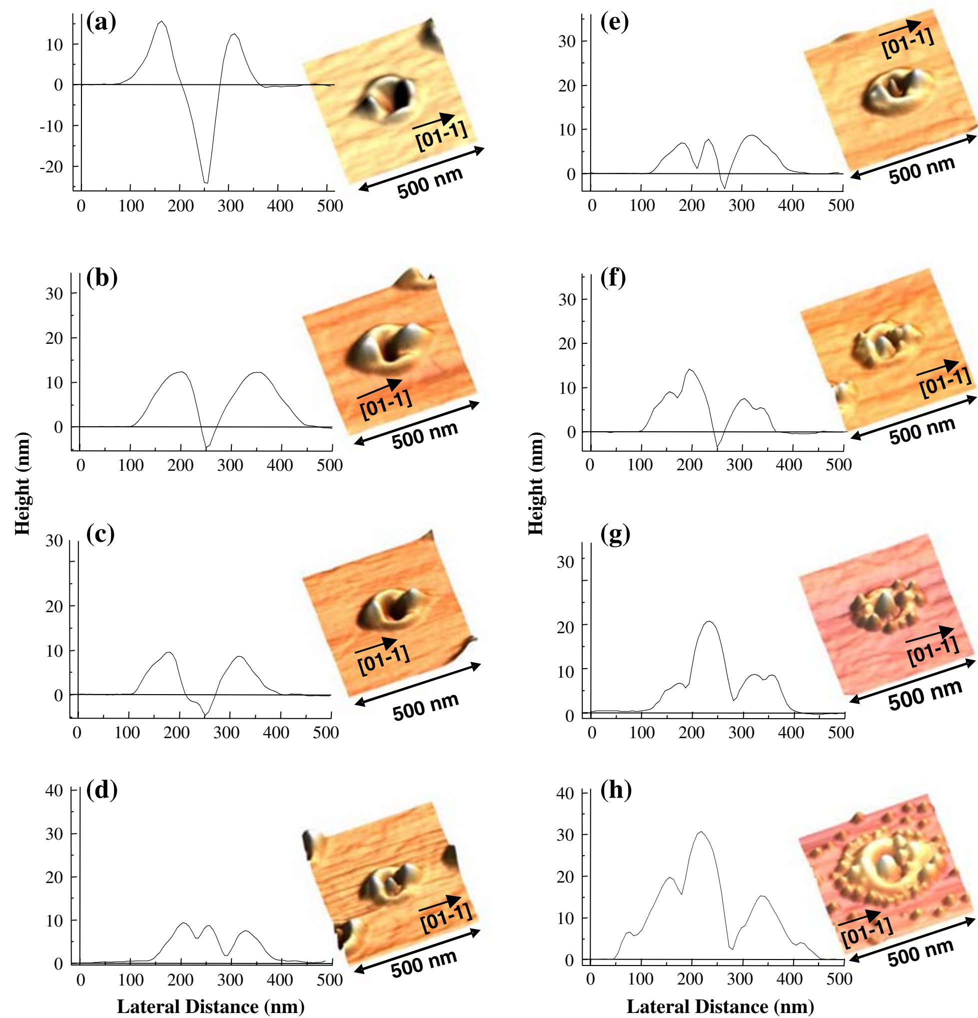

Fig. 2 Cross-sectional profiling as well as 3 D rendering of the nanostructure morphologies in each sample from Fig. 1: (**a**) 0.0 ML, (**b**) 0.8 ML, (**c**) 1.2 ML, (**d**) 1.36 ML, (**e**) 1.6 ML, (**f**) 1.76 ML, (**g**) 2.0 ML, and (**h**) 2.4 ML. Each specifically shows the main QD's profile and the variations in heights and morphologies of the ring-like nanostructures and QDs. Data scales are ~40 nm × 500 nm, with the height scales zeroed approximately at the reconstructed surface

deposition. At the last stage, the center InAs QDs may be dislocated and become the trap center around InAs materials.

Photoluminescent (PL) measurements were taken on a sample with 1.2 ML InAs deposition, capped with 200 ML GaAs, and it seems to display unique features.

Table 1 Distributions and average dimensions for each InAs coverage

ML deposition	Mean QD height (nm)[a]	Mean QD diameter nm)	QD aspect ratio[b]	QD density per QR[c]	QD density cm^{-2})[d]	Mean depth of hole (nm)[e]
0.0	–	–	–	0	0	22.1 (±3.7)
0.8	–	–	–	0	0	5.3 (±2.0)
1.2	3.1 (±1.3)	33.8 (±7.8)	10.9	~1.0	~5.5 × 10^{8}	4.7 (±1.6)
1.36	6.0 (±1.0)	49.2 (±7.0)	8.2	~1.1	~5.5 × 10^{8}	6.6 (±1.7)
1.6	10.4 (±1.5)	55.3 (±4.4)	5.3	~1.5	~5.5 × 10^{8}	9.5 (±3.1)
1.76	19.2 (±2.1)	79.8 (±5.1)	4.2	~7	~4 × 10^{9}	5.8 (±2.9)
2.0	18.7 (±3.3)	87.3 (±10.8)	4.7	~13	~7 × 10^{9}	3.3 (±2.1)
2.4	30.2 (±3.2)	107.9 (±10.2)	3.6	~27	~2 × 10^{10}	2.1 (±4.0)

[a] Height of the main QD above the hole (or reconstructed surface in the 1.6–2.4 ML depositions)

[b] Diameter to height aspect ratio

[c] Number of QDs per ring-like nanostructure, including each QD in and around the perimeter of the ring-like nanostructure

[d] Density of QDs on the sample

[e] Depth of the hole below the reconstructed surface

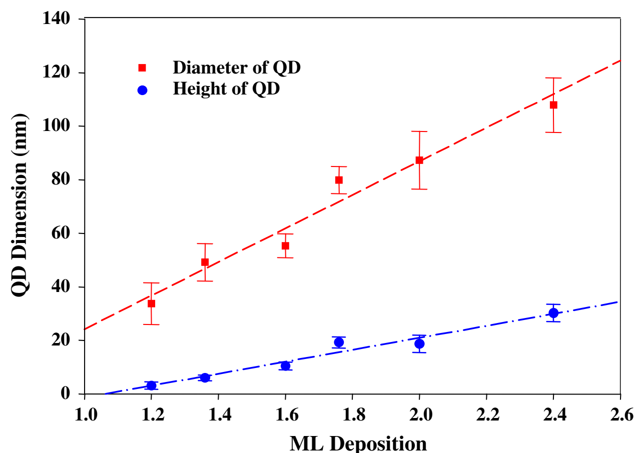

Fig. 3 A plot of the main QD dimensions, showing the somewhat linear progression of the height and diameters with increased ML deposition

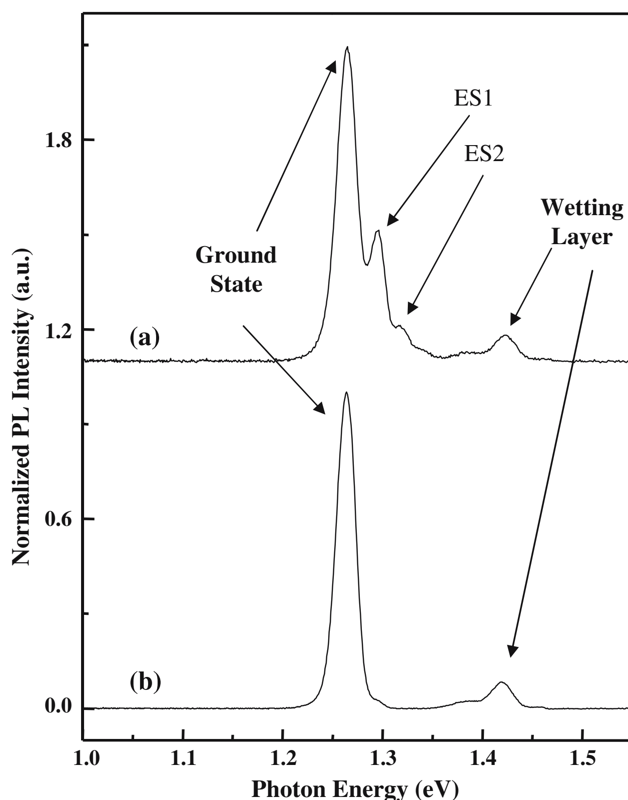

Fig. 4 PL measurements for different 532 nm-wavelength laser excitations at 10 K on a 1.2 ML InAs deposition sample, with the ground state, wetting layer, and first (ES1) and second (ES2) excited states labeled. The normalized PL intensity curves are at a laser power density of (**a**) 40 W/cm^2 and (**b**) 1.26 W/cm^2

Figure 4a shows the normalized PL curve of a 532 nm wavelength lasing of this sample at a power density of 40 W/cm^2, and Fig. 4b shows the curve at a lasing power density of 1.26 W/cm^2, both at 10 K. The peak of this sample's curve at 1.26 W/cm^2 excitation in Fig. 4b is centered at 1.264 eV, and the full-width half-maximum (FWHM) is 22.3 meV, less than the FWHM of the PL of typical InAs QDs [26]. Also, there is negligible shift in energy in the ground state curve peak when the excitation was increased to 40 W/cm^2, giving an indication that QDs retain the same energy states for the ground state excitonic recombinations. The other excited states are labeled in Fig. 4. Thus, this 1.2 ML coverage sample displays good QD homogeneity, which indicates that this form of InAs QD growth on Ga droplet templates may have potential in optoelectronics.

Conclusion

Using MBE, we combined droplet homo-epitaxy and SK-growth techniques to self-assemble InAs QDs on GaAs ring-like nanostructures. The progression of the InAs QD formation on these template GaAs ring-like structures is demonstrated. Increased deposition of InAs on the ring-like nanostructures first produced a QD in the hole followed QDs around the GaAs ring and on the GaAs (100) surface. The large QDs showed good uniformity and a unique progression in size with the increased ML coverage. This method of InAs QD formation may have potential applications in optoelectronics and motivate further research into other types of QD and nanostructure configurations.

Acknowledgments The authors thank Dr. John Shultz for his strong support in the facility maintenance and the financial support of the NSF (through Grant DMR-0520550). The WSxM© **image processing program was used in this paper (http://www.nanotec.es).**

References

1. S.-S. Li, G.-L. Long, F.-S. Bai, S.-L. Feng, H.-Z. Zheng, Pro. Natl. Acad. Sci. USA, **98**(21), 11847 (2001); S. Chutia, M. Friesen, R. Joynt, Phys. Rev. B **73**, 241304(R) (2006)
2. M. Sugawara, K. Mukai, Y. Nakata, H. Ishikawa, A. Sakamoto, Phys. Rev. B **61**, 7595 (2000)
3. R.M. Thompson, R.M. Stevenson, A.J. Shields, I. Farrer, C.J. Lobo, D.A. Ritchie, M.L. Leadbeater, M. Pepper, Phys. Rev. B **64**, 201302(R) (2001)
4. Z. Yuan, B.E. Kardynal, R. Mark Stevenson, A.J. Shields, C.J. Lobo, K. Cooper, N.S. Beattie, D.A. Ritchie, M. Pepper, Science **295**, 102 (2002)
5. D.C. Unitt, A.J. Bennett, P. Atkinson, D.A. Ritchie, A.J. Shields, Phys. Rev B **72**, 33318 (2005)
6. M. Kroutvar, Y. Ducommun, J.J. Finley, M. Bichler, G. Abstreiter, A. Zrenner, Appl. Phys. Lett. **83**, 443 (2003)

7. A.J. Shields, M.P. O'Sullivan, Appl. Phys. Lett. **76**, 3673 (2000)
8. N. Pradhan, D. Goorskey, J. Thessing, X. Peng, J. Am. Chem. Soc. **127**, 17586 (2005)
9. J.H. Lee, Zh.M. Wang, B.L. Liang, W.T. Black, V.P. Kunets, Y.I. Mazur, G.J. Salamo, Nanotechnology **17** 2275 (2006)
10. Z. Sun, B. Yang, Nanoscale Res. Lett. **1,** 46 (2006)
11. Zh.M. Wang, J.H. Lee, B.L. Liang, W.T. Black, V.P. Kunets, Y.I. Mazur, G.J. Salamo, Appl. Phys. Lett. **88**, 233102 (2006)
12. S. Kohmoto, H. Nakamura, T. Ishikawa, K. Asakawa, Appl. Phys. Lett. **75**, 3488 (1999)
13. H.Z. Song, T. Usuki, T. Ohshima, Y. Sakuma, M. Kawabe, Y. Okada, K. Takemoto, T. Miyazawa, S. Hirose, Y. Nakata, M. Takatsu, N. Yokoyama, Nanoscale Res. Lett. **2**, 160 (2006)
14. K.P. Chang, S.L. Yang, D.S. Chuu, R.S. Hsiao, J.F. Chen, J. Appl. Phys. **97**, 83511 (2005); E. Ribeiro, E. Muller, T. Heinzel, H. Auderset, K. Ensslin, G. Medeiros-Ribeiro, P.M. Petroff, Phys. Rev. B **58**, 1506 (1998)
15. H. Shin, J.B. Kim, Y.H. Yoo, W. Lee, E. Yoon, Y.M. Yu, J. Appl. Phys. **99**, 023521 (2006); M. Henini, Nanoscale Res. Lett. **1,** 32 (2006)
16. N. Koguchi; K. Ishige, Jpn. J. Appl. Phys. **32**(5A), 2052 (1993); T. Mano, T. Kuroda, S. Sanguinetti, T. Ochiai, T. Tateno, J. Kim, T. Noda, M. Kawabe, K. Sakoda, G. Kido, N. Koguchi, Nano Lett. **5**, 425 (2005)
17. S.Y. Lehman, R. Alexana, R.P. Mirin, J.E. Bonevich, Mater. Res. Soc. Symp. – Proc., **737**, 179 (2003); Y.H. Chen, X.L. Ye, Z.G. Wang, Nanoscale Res. Lett. **1**, 79 (2006)
18. T. Lundstrom, W. Schoenfeld, H. Lee, P.M. Petroff, Science **286**, 2312 (1999)
19. R. Songmuang, S. Kiravittaya, O.G. Schmidt, Appl. Phys. Lett. **82**, 892 (2003)
20. R.J. Warburton, C. Schäflein, D. Haft, F. Bickel, A. Lorke, K. Karrai, J.M. Garcia, W. Schoenfeld, P.M. Petroff, Nature **405**, 926 (2000)
21. M. Volmer, A. Weber, Z. Phys. Chem. **119,** 277 (1926)
22. Z.M. Wang, K. Holmes, J.L. Shultz, G.J. Salamo, Phys. Stat. Sol. (a) **202**, R85 (2005)
23. Z. Gong, Z.C. Niu, S.S. Huang, Z.D. Fang, B.Q. Sun, J.B. Xia, Appl. Phys. Lett. **87**, 93116 (2005)
24. H.S. Djie, O. Gunawan, D.-N. Wang, B.S. Ooi, J.C.M. Hwang, Phys. Rev. B **73**, 155324 (2006)
25. F. Patella, M. Fanfoni, F. Arciprete, S. Nufris, E. Placidi, A. Balzarotti, F. Patella, et al., Appl. Phys. Lett. **78**, 320 (2001)
26. S. Godefroo, J. Maes, M. Hayne, V.V. Moshchalkov, M. Henini, F. Pulizzi, A. Patanè, L. Eaves, J. Appl. Phys. **96**, 2535 (2005)